A Novel 3-D Scattering Model of 1.8-GHz Radio Propagation in Microcellular Urban Environment

J. H. Tarng, *Member, IEEE,* and K. M. Ju

***Abstract*—This work presents a novel three-dimensional (3-D) scattering model to predict the path loss of a microcellular radio channel in an urban environment. The analytical scattering model combined with a patched-wall model predicts the median path loss more accurately than the conventional analytical ray-tracing model in the cases studied. Comparing the path loss with the measured one at 1.8 GHz demonstrates the effectiveness of the scattering model. The scattering model includes three major propagation modes: 1) a direct-path wave; 2) a ground-reflected wave; and 3) the scattered field from the walls aligned along a street. The proposed model with a polarization scattering matrix associated with the patched-wall model aptly describes the third mode, which is usually neglected or oversimplified.**

***Index Terms*—Microcellular measurement, radio channel modeling, ray-tracing technique, scattering cross section.**

I. Introduction

THE tremendous growth of cellular mobile radio and the anticipated need for personal communications will create a need for additional communication channels, particularly in densely populated urban areas. The capacity improvement through additional cell splitting in the present generation of cellular radio systems has practical limits because of antenna site constraints. An alternative approach is to use a microcellular structure. Therefore, microcellular systems, such as PHS, DECT, PACS, and CT2 have been introduced in urban or indoor environments [1], [2]. System designers wishing to design a system with optimal frequency assignment and reuse must study in detail microcellular channel characteristics such as median path loss, channel fading, and pulse delay and spread. There are many investigations describing related research [3]–[14].

In this paper, a novel site-specific scattering model is developed for the microcellular channels in urban environment. The analytical scattering model, combined with a patched-wall model, predicts the median path loss more accurately than the conventional analytical ray-tracing model in the cases studied. The patched-wall model has been used to model an indoor radio channel using patches of different dielectric constants and sizes to model indoor walls and boundaries [15]. These patches were assumed to have infinite size in computing the corresponding reflected field and formulas of the Fresnel reflection coefficients are employed. The formulas are true only when the size of the reflecting patch is much larger than the wavelength of incident wave. The assumption may not be valid in microcellular environments where the structures and materials of street walls vary from door to door. Therefore, it is more proper to treat each patch as a finite-size scatterer, as in this investigation. This paper evaluates the scattering cross section matrix to determine the corresponding scattered field [16], [17]. The work computes not only the field scattered from the street walls, but also the effect on the received field of the ground-reflected wave and the direct wave. To our knowledge, other studies employ radar cross section (RCS) to explore the energy scattered from building walls or terrain pixels [18]–[21].

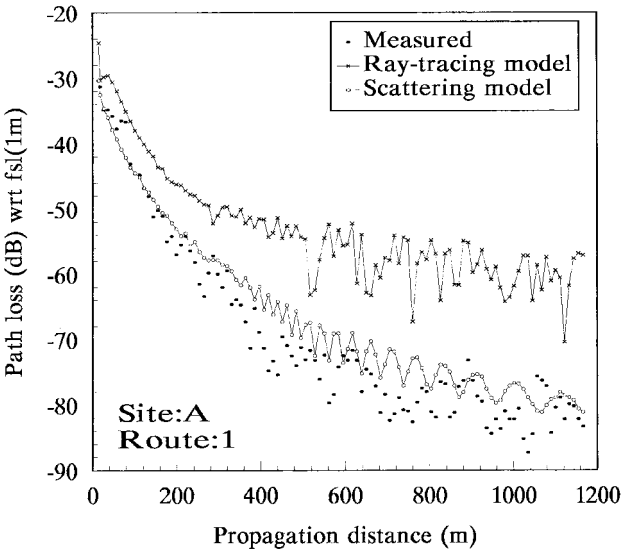

Fig. 1. The measured and computed path losses that are relative to the path loss in free-space at 1 m are illustrated as a function of propagation distance. The path losses are measured along route 1 of site A.

Several models use analytical ray-tracing techniques to predict microcellular radio channels [3]–[9], [15]. Most of these models assume that street walls are smooth flat surfaces with average (effective) relative permittivity (ε_r) and conductivity (σ). This assumption neglects the scattering and absorption natures of the wall. Fig. 1 presents the prediction error that can result from this assumption by comparing the measured and computed median path losses for 1.8-GHz radio along

Manuscript received April 13, 1998; revised February 5, 1999. This work was supported in part by the National Science Council of Taiwan under Projects NSC87-2213-E-009-148 and NSC88-2213-E-009-110.

The authors are with the Department of Communications Engineering, Chiao-Tung University, Hsin-Chu, Taiwan, R.O.C.

Publisher Item Identifier S 0018-9375(99)04085-5.

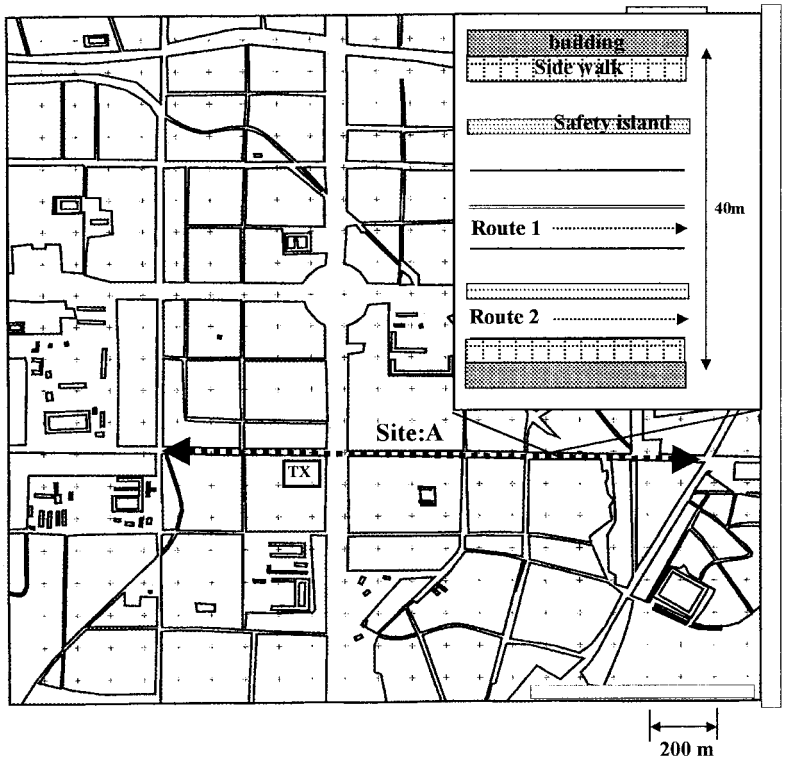

Fig. 2. Map of measurement site A and the layout of the measured streets.

a street in eastern Taipei (shown in Fig. 2). The direct path between the transmitter and the receiver is clear (line-of-sight propagation) for all measured points. The following sections describe other details related to the measurement. The difference between the computed and measured losses increases as the propagation distance increases beyond 100 m. This difference is mainly due to the many strong reflected rays introduced by the smooth flat surface and averaged material model that in reality may be absorbed or scattered away. The ray-tracing model may overestimate received power because of these nonexistent reflected rays, especially for long propagation ranges. The patched-wall scattering model eliminates this discrepancy as shown by the computed result in Fig. 1. Further comparisons between the measured and the computed losses shown in Section IV prove the capability of the model proposed in this study.

II. Propagation Environment, Measurement Procedure, and Patched-Wall Model

A. Measurement Procedure and Sites

Narrow-band (CW) signal strength measurements were made at 1.8 GHz at three sites. Site A, is located in eastern Taipei City; sites B and C, are in Chung-Li, a small city about 40 km from Taipei. During the investigation, a half-wavelength dipole antenna transmitted a 37-dBm CW signal; the antenna was sited 6 m above the ground, mounted on a measuring pole that was tied to a tree near the sidewalk. The receiving antenna, a half-wavelength dipole antenna, was mounted on the rooftop of a test van, which was moving along a roadway; its height was 1.7 m above ground. A PC-controlled receiver (Rohde and Schwarz ESVP-52), equipped with a downconverter, continuously sampled the received power along each measured route every half wavelength. For each measured point, 100 samples taken within a distance of 50 wavelengths determined the measured median power in that distance. There were 780, 343, and 166 measured points for the routes at sites A, B, and C, respectively. The measured routes for these sites are shown in Figs. 2 and 3. The roads at sites A, B, and C are 40, 25, and 15 m wide, respectively. The average heights of the buildings along routes at sites A, B, and C are 30, 18, and 12 m, respectively. These routes are carefully chosen in order to include proper characteristics of local environments. All the measured points on these routes allow line-of-sight propagation between the transmitting and receiving antennas.

B. Patched-Wall Model

Construction features and constitutive materials of street walls for urban cities are complicated and may vary from door to door. This large variation leads to a wide range of reflectivity or scattering property along each street. Using "average building material" to represent the average effect of the constitutive materials of the street walls may be a practical method. However, the permittivity of the average material is not easy to determine since it depends on the measured data as well as the propagation model [6], [22]. In this study, patches of different dielectric constants and sizes model the street walls according to their physical structure and dimension. Since the sizes of these patches are finite, they will scatter instead of reflect the incident field. Therefore, in this

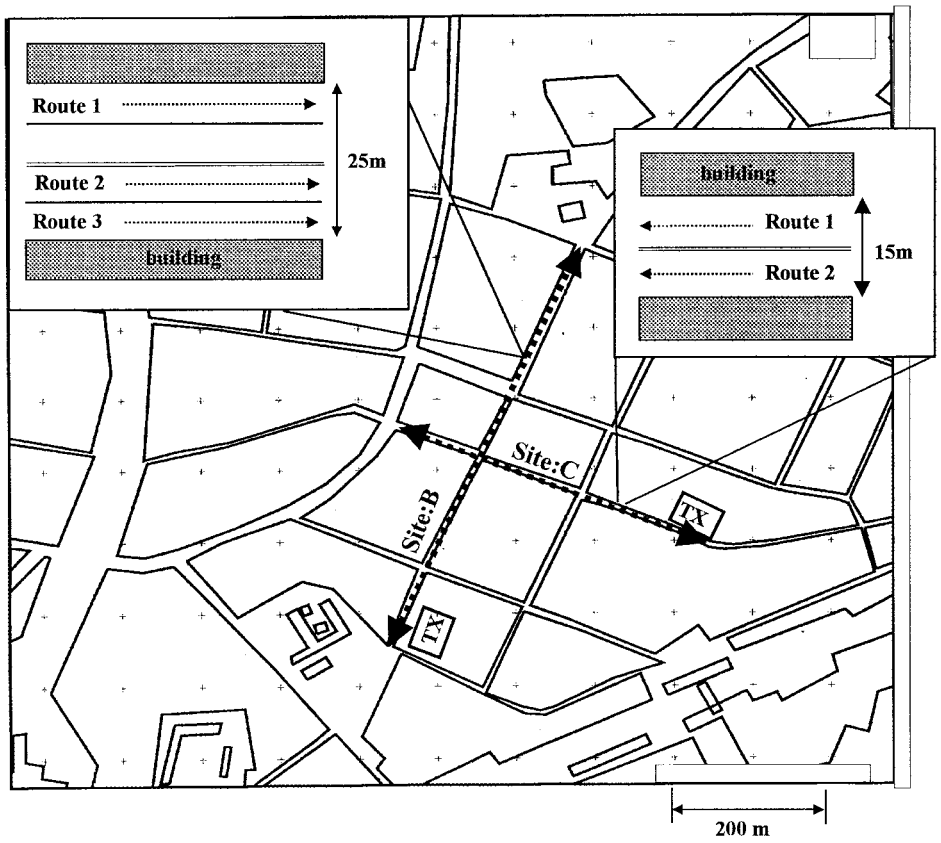

Fig. 3. Map of measurement sites B and C, and the layout of the measured streets.

Fig. 4. Typical street buildings at site A.

work, a patched-wall scattering model describes the scattering field due to each patch. For example, Fig. 4 illustrates typical construction features of buildings at site A. Since the features of the buildings along the both streets are similar, they are modeled as an uniform array of construction or building unit, which is shown in Fig. 5(a). The building unit of the street buildings is simplified and modeled using three different patches: Fig. 5(b) displays the results. The absorber patch models the complicated surface features such as the first-floor shop fronts that will trap or diffuse the incident wave. The window patch models the windows in each building. The concrete patch describes the concrete walls of each building. According to the Rayleigh criterion, the surface of street buildings, which is slightly rough, can be viewed as a smooth surface. Each scattering patch is modeled according to its average surface property. Fig. 6(a) illustrates typical construction features of the street buildings at site B. Since construction features of the buildings along the streets at site B resemble those at site A, site A patches with different sizes also model the buildings at site B. The modeling result is shown in Fig. 6(b). The model shown in Fig. 6(b) also describes the buildings at site C since the buildings at sites B and C are similar. The uniform array of patches presented in Fig. 5(a) also model the buildings at site B or site C but with different sizes.

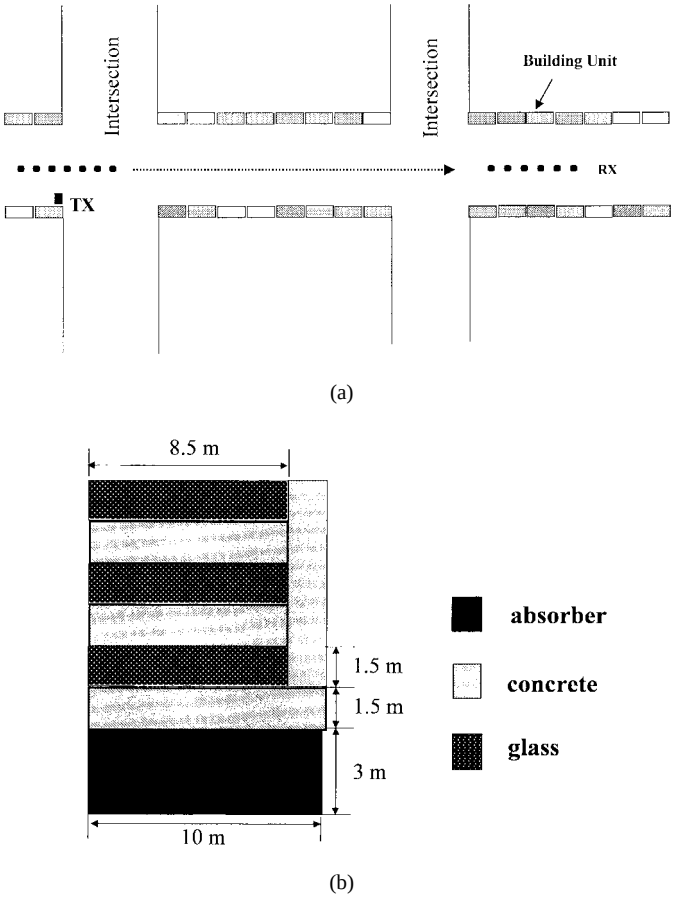

Fig. 5. Layout of site A. (a) Top view. (b) Front view of each building unit.

III. Propagation Model

The proposed model includes three major propagation modes: 1) a direct-path wave $\vec{E}_D$; 2) a ground-reflected wave $\vec{E}_G$; and 3) the scattered fields from the walls aligned along the streets $\vec{E}_S$. Summation of these waves determines the receiving field at an observation position and yields

$$\vec{E}_R = \vec{E}_D + \vec{E}_G + \vec{E}_S. \tag{1}$$

The ground-reflected wave is given by

$$\vec{E}_G = \vec{E}_o G_t G_r L_f(d) R_g(\theta_g) \tag{2}$$

where $\vec{E}_o$ is the field 1 m away from the transmitting antenna. G_t and G_r are the field amplitude radiation patterns of the transmitting and the receiving antennas, respectively. $L_f(d) = e^{-jkd}/4\pi d$ is the free-space propagation factor with an unfolded path length d. $R_g(\theta_g)$ is the Fresnel reflection coefficient of ground with an incident angle θ_g. It is noted that the expression of $\vec{E}_D$ can be obtained from (2) by setting $R_g = 1$.

The vector field $\vec{E}_S$ is equal to the summation of all the scattered fields from every patch of the both walls aligned along the measured street and is given by

$$\vec{E}_S = \sum_{j=1}^{m} \vec{E}_j^s. \tag{3}$$

The jth scattered field $\vec{E}_j^s$ at the observation position is due to the incident field $\vec{E}_j^i$ scattered by the jth patch is given by

$$\begin{bmatrix} E^S_{\alpha 2} \\ E^S_{\beta 2} \end{bmatrix}_j = \begin{bmatrix} S_{11} & S_{12} \\ S_{21} & S_{22} \end{bmatrix}_j \begin{bmatrix} E^i_{\alpha 1} \\ E^i_{\beta 1} \end{bmatrix}_j \tag{4}$$

where $[S]$ is the polarization scattering matrix (PSM) [17]. It is noted that a ray-fixed coordinate system has already been introduced to reduce the scattering matrix from a 3×3 matrix (in a global coordinate system) to a 2×2 matrix whose elements are much easier to determine. Using the ray-fixed coordinate systems, the incident or the scattered field has been decomposed into two independent polarizations. In Fig. 7, the incident and scattered ray-fixed coordinates are shown and represented by $(\hat{d}_1, \hat{\alpha}_1, \hat{\beta}_1)$ and $(\hat{d}_2, \hat{\alpha}_2, \hat{\beta}_2)$, respectively. The direction of propagation and the normal unit vector of the scattering boundary determine the coordinate axes of these local coordinate systems. Determination of these vectors can be found in another work [15].

The incident field arriving at the jth patch $\vec{E}_j^i$ is given by

$$\vec{E}_j^i = \vec{E}_o G_{tj} L_f(d_{Tj}) \tag{5}$$

where $L_f(d_{Tj}) = e^{-jkd_{Tj}}/4\pi d_{Tj}$ and G_{tj} is the field-amplitude radiation pattern of the antenna. d_{Tj} represents the distance between the transmitting antenna and the center of the jth patch.

The component of the PSM due to the jth patch S_{lk} is related to the corresponding RCS σ_{lk} by

$$S_{lk} = \frac{\sqrt{\sigma_{lk}}}{\sqrt{4\pi}\, d_{sj}} \tag{6}$$

where d_{Sj} is the distance between the jth patch center and the observation position and l, $k = 1$, or 2. For a rectangular

(a)

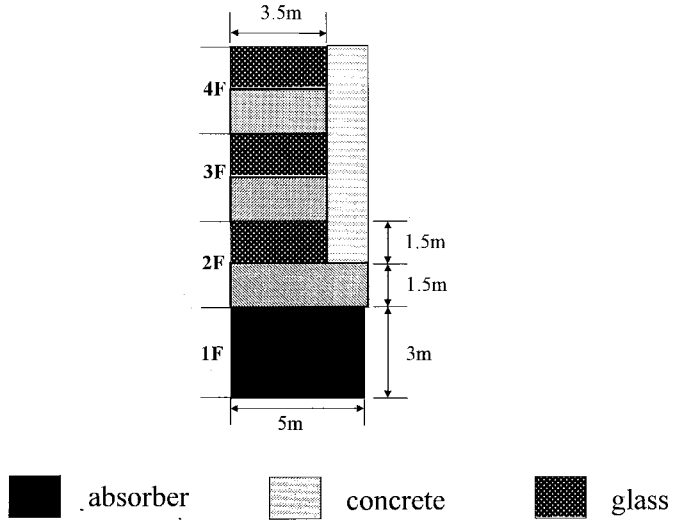

(b)

Fig. 6. (a) Typical street buildings at site B. (b) The building unit at site B is modeled and represented by three kinds of patches.

patch ($L_x \times L_y$), as shown in Fig. 5, σ_{lk} is given by [16] where

$$\sigma_{lk} = \frac{k^2}{\pi}(L_x L_y)^2 \left(\frac{\sin k\xi_x L_x/2}{k\xi_x L_x/2}\right)^2 \left(\frac{\sin k\xi_y L_y/2}{k\xi_y L_y/2}\right)^2 |\gamma_{lk}|^2 \tag{7}$$

$$\xi_x = \sin\theta_i - \sin\theta_s \cos\varphi_s,$$
$$\xi_y = \sin\theta_s \sin\varphi_s,$$
$$\gamma_{11} = \cos\theta_i \cos\varphi_s R_s(\theta_i),$$
$$\gamma_{12} = \sin\varphi_s R_p(\theta_i),$$

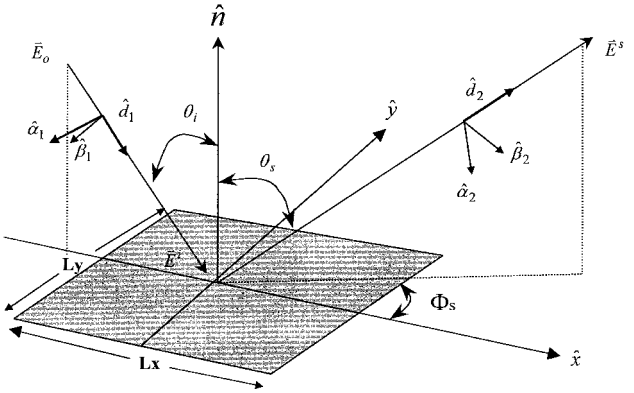

Fig. 7. The ray-fixed coordinate systems associated with the scattering at a rectangular plate.

$$\gamma_{21} = \cos\theta_i \cos\theta_s \sin\varphi_s R_s(\theta_i),$$
$$\gamma_{22} = -\cos\theta_i \cos\varphi_s R_p(\theta_i).$$

θ_i is the incident angle and θ_S is the scattering angle on the plane defined by $\phi = \phi_S$ shown in Fig. 7. $R_S(\theta)$ and $R_p(\theta)$ are the Fresnel reflection coefficients of the patch for the polarizations perpendicular and parallel to the plane of incidence, respectively. Their formulations are given in another work [15].

It is noted that in the use of the scattering model the propagation range is limited due to the assumption that the incidence field has to be a uniform plane wave, or nearly so. This is the far-field approximation and the area of the patch L_xL_y should be less than $\lambda \cdot d_s/2$, where d_s is the distance between the receiving antenna and the center of the scattering patch. However, this upper bound will be relaxed if the average or median values of the scattered area is desired, which satisfies the propagation scenarios here, and then it becomes $d_S d_T \gg L_xL_y$ [16].

IV. Numerical Simulation and Comparison

This study averages the sampled path loss, computed by either model, over a length of 50 wavelengths, to compute the median path loss. The value of (ε_r, σ) of the concrete and ground used to compute the RCS is the same as the average value used for the 3-D ray-tracing model; these values are (3, 0.005) and (15, 7) [5], respectively. Note that the averaged (ε_r, σ) of the glass is equal to (7, 10^{-12}) [23].

The ray-tracing model can include the direct, reflected, and refracted (transmitted) fields that the rays represent. Each propagation mode is treated separately. The 3-D ray-tracing model used in this study considers direct, ground-reflected, and wall-reflected fields as the dominant modes for radio propagation along a street in microcellular environment. The receiver may receive many wall-reflected rays; the vector field of the ith wall-reflected ray at the receiver is given by

$$\vec{E}_i = \vec{E}_o G_{ti} G_{ri} L_f(d) \prod_j \overline{\overline{R}}(\theta_{ji}) \tag{8}$$

where $\overline{\overline{R}}(\theta_{ji})$ is the reflection coefficient of the ith received ray at jth reflection with incident angle θ_{ji}. To simplify the calculation of the reflection coefficient, the ray-fixed coordinate systems are also employed [15]. It is noted that the number of reflections is determined by two factors: 1) when ray intensity falls below a specified threshold and 2) when the received field envelope converges. The numerical simulation in this study uses five reflections.

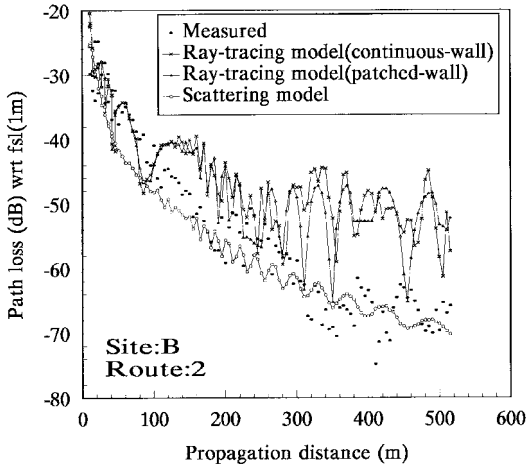

Fig. 8. The measured and computed path losses for route 2 of site B. The ray-tracing model using the patched-wall model is also employed for comparison.

In Fig. 1, the median path loss computed by the 3-D ray tracing model or the scattering model is compared with the measured median path loss in Taipei City. The scattering model performs better than the 3-D model, especially in the far range; it also spends less computing time. Additional comparisons between the computed and the measured losses at sites B and C conformed the accuracy of the scattering model, as shown in Fig. 3. The investigation measured the transmitted signals on routes along the street at both sites. In Figs. 8 and 9, the computed and measured path losses are shown for sites B and C, respectively; the scattering model performs consistently well, while the 3-D ray-tracing model yields poor prediction accuracy in the far range. Fig. 8 also displays the path loss computed by using the ray-tracing model combined with the patched-wall model shown in Fig. 4(b). This combination yields slightly better prediction accuracy than the ray-tracing model combined with the continuous-wall model, but does not predict as well as the scattering model. To quantify the comparison result, the mean of the error m_e and the standard deviation of the error σ_e are defined and computed. The error e represents the difference between the computed and measured path losses. In Table I, values of m_e and σ_e for each route at sites A, B, and C are given. It is found that the scattering model performs well at these sites. The largest error (at site A) may be due to neglecting the effect of many local scatterers such as moving traffic, trees, and pedestrians near or along the propagation paths.

V. Summary

A novel 3-D scattering model is developed and shown to have a reasonable prediction accuracy for 1.8-GHz radio wave propagation along a street in microcellular environment. The

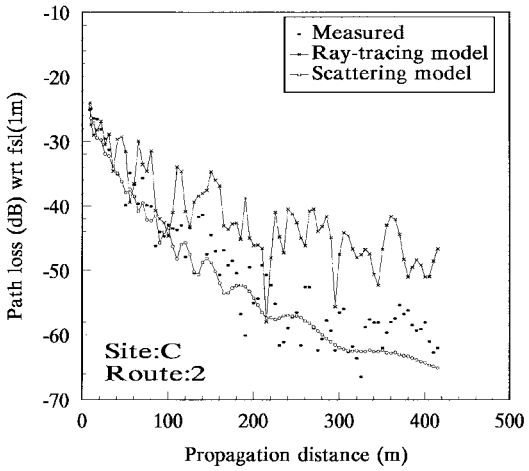

Fig. 9. The measured and computed path losses for route 2 of site C.

scattering model describes the scattered field from the street walls more accurately than the traditional ray-tracing model when the propagation range is large. The ray-tracing model predicts strong reflections due to waveguide effect caused by the street layout, leading to the prediction of high power in the far region. In reality, some of the reflected power is scattered in other directions, so that the actual waveguide effect is less than the predicted effect, leading to lower far-region power levels. The scattering model proposed in this study this scattered power into account, and thereby results in predicted far-region power which is lower than that predicted by the ray tracing model, consequently resulting in a better agreement with measurements.

REFERENCES

[1] R. Steele and V. K. Prabu, "High-user-density digital cellular mobile radio system," *Proc. Inst. Elect. Eng.*, vol. 132, pt. F, pp. 396–404, Aug. 1985.
[2] H. Hashemi, "The indoor radio propagation channel," *Proc. IEEE*, vol. 81, pp. 943–968, July 1993.
[3] A. J. Rustako, Jr., N. Amitay, G. J. Owens, and R. S. Roman, "Radio propagation at microwave frequencies for line-of-sight microcellular mobile and personal communications," *IEEE Trans. Veh. Technol.*, vol. 40, pp. 203–210, Feb. 1991.
[4] K. R. Schaubach, N. J. Davis, and T. S. Rappaport, "A ray tracing method for predicting path loss and delay spread in microcellular environments," in *Proc. Veh. Technol. Conf.*, Denver, CO, May 1992, pp. 932–935.
[5] A. G. Kanatas, I. D. Kountouris, G. B. Kostaras, and P. Constantinou, "A UTD propagation model in urban microcellular environments," *IEEE Trans. Veh. Technol.*, vol. 46, pp. 185–193, Feb. 1997.
[6] S. Y. D. Tan and H. S. Tan, "A theory for propagation path-loss characteristics in a city-street grid," *IEEE Trans. Electromagn. Compat.*, vol. 37, pp. 333–342, Aug. 1995.
[7] V. Erceg, A. J. Rustako, and R. S. Roman, "Diffraction around corners and its effects on the microcell coverage area in urban and suburban environments at 900 MHz, 2 GHz, and 6 GHz," *IEEE Trans. Veh. Technol.*, vol. 43, pp. 762–766, Aug. 1994.
[8] K. Rizk, J.-F. Wagen, and F. Gardiol, "Two-dimensional ray-tracing modeling for propagation prediction in microcellular environments," *IEEE Trans. Veh. Technol.*, vol. 46, pp. 508–517, May 1997.
[9] N. Amitay, "Modeling and computer simulation of wave propagation in lineal line-of-sight microcells," *IEEE Trans. Veh. Technol.*, vol. 41, pp. 337–342, Nov. 1992.
[10] J. H. Whitteker, "Measurements of path loss at 910 MHz for proposed microcell urban mobile systems," *IEEE Trans. Veh. Technol.*, vol. 37, pp. 125–129, Aug. 1988.
[11] R. J. C. Bultitude and G. K. Bedal, "Propagation characteristics on microcellular urban mobile radio channel at 910 MHz," *IEEE J. Select. Areas Commun.*, vol. 7, pp. 31–39, Jan. 1989.
[12] N. Feng and H. Bertoni, "Path loss and cell coverage of urban microcells in high-rise building environments," in *Proc. GLOBECOM'93*, Phoenix, AZ, Nov. 1993, pp. 266–270.
[13] K. R. Schaubach and N. J. David, IV, "Microcellular radio-channel propagation prediction," *IEEE Antennas Propagat.*, vol. 36, pp. 25–34, Jan. 1994.
[14] S. Kozono and A. Taguchi, "Mobile propagation loss and delay spread characteristics with a low base station antenna on an urban road," *IEEE Trans. Veh. Technol.*, vol. 42, pp. 103–109, Feb. 1993.
[15] J. H. Tarng, W. R. Chang, and B. J. Hsu, "Three-dimensional modeling of 900-MHz and 2.44-MHz radio propagation in corridors," *IEEE Trans. Veh. Technol.*, vol. 46, pp. 519–527, May 1997.
[16] G. T. Ruck, D. E. Barrick, W. D. Stuart, and C. K. Krichbaum, *Radar Cross Section Handbook.* New York: Plenum, 1970, vol. II.
[17] E. F. Knott, J. F. Shaeffer, and M. T. Tuley, *Radar Cross Section*, 2nd ed. Norwood, MA: Artech House, 1993.
[18] T. Kurner, D. J. Cichon, and W. Wiesbeck, "Concepts and results for 3D digital terrain-based wave propagation models: An overview," *IEEE J. Select. Areas Commun.*, vol. 11, pp. 1002–1012, Sept. 1993.
[19] E. K. Tameh, A. R. Nix, and M. A. Beach, "3-D integrated macro and microcellular propagation model, based on the use of photogrammetric terrain and building data," in *IEEE Veh. Technol. Conf.*, Phoenix, AZ, May 1997, pp. 1957–1961.
[20] U. Liebenow and P. Kuhlmann, "A three-dimensional wave propagation model for macrocellular mobile communication networks in comparison with measurements," in *IEEE Veh. Technol. Conf.*, Atlanta, GA, Apr. 1996, pp. 1623–1627.
[21] S. Y. Seidel, T. S. Rappaport, S. Jain, M. L. Lord, and R. Singh, "Path loss, scattering, and multipath delay statistics in four European cities for digital cellular and microcellular radiotelephone," *IEEE Trans. Veh. Technol.*, vol. 40, no. 4, pp. 721–730, Nov. 1991.
[22] S. Y. Seidel and T. S. Rappaport, "Site-specific propagation prediction for wireless in-building personal communication system design," *IEEE Trans. Veh. Technol.*, vol. 43, no. 4, pp. 879–891, Nov. 1994.
[23] D. K. Cheng, *Field and Wave Electromagnetics*, 2nd ed. New York: Addison-Wesley, 1989.

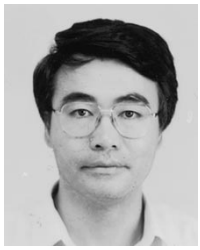

J. H. Tarng (S'85–M'89) received the B.S. degree in power mechanical engineering from National Tsin-Hua University, Hsin-Chu Taiwan, R.O.C., in 1981, and the M.S. and Ph.D. degrees in electrical engineering from Pennsylvania State University, University Park, in 1988 and 1989, respectively.

He is currently a faculty member in the Department of Communication Engineering at National Chiao Tung University, Hsin-Chu. His research interests include radio propagation and modeling and measurement, wireless communications, and electromagnetic compatibility.

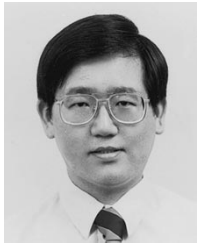

K. M. Ju received the B.S. and M.S. degrees in atmospherical physics from National Central University, Chung-Li, Taiwan, R.O.C., in 1980 and 1982, respectively. He is currently working toward the Ph.D. degree in the Department of Communication Engineering at National Chiao-Tung University, Hsin-Chu, Taiwan, R.O.C.

His research interests include radio propagation modeling for cellular and microcellular communications.